Reprinted from
THE PHYSICS OF FLUIDS
Volume 11, Number 10, October 1968

Stability of Parallel Flow between Concentric Cylinders

J. E. MOTT* AND D. D. JOSEPH
Institute of Technology, University of Minnesota, Minneapolis, Minnesota
(Received 12 September 1966; final manuscript received 6 June 1968)

The linear stability of parallel flow in a concentric annulus to infinitesimal, axially symmetric disturbances is considered. First, the Poiseuille flow in annular cylinders is studied with the ratio k of the outer to inner cylinder as a parameter. The critical Reynolds number is a monotone function of this radius ratio, increasing without bound as $k \to \infty$ (Hagen–Poiseuille flow) from the plane Poiseuille flow limit ($k = 1$). Second, a one-parameter family of skewed (variable viscosity) flows in a fixed annulus is studied. The neutral curves for many of these skewed profiles have a second minimum, which for sufficiently skewed profiles, gives the lowest value of the Reynolds number. These two minima are associated with two very different distributions of Reynolds stress. Both distributions are such that on part of the channel the energy is transferred from the disturbance motion to the basic motion and both can be explained by analysis of the Reynolds stress jump condition and the known structure of Reynolds stress near a rigid wall.

I. INTRODUCTION

Two very well-known and seemingly paradoxical results of the linear theory of stability pertain to Poiseuille motions in round pipes and plane channels.[1] The plane-Poiseuille motion is definitely unstable for Reynolds numbers in excess of about 6000.[2] However, every linear analysis of the pipe (Hagen–Poiseuille) motion has concluded for absolute stability.[3,4] It is with these results in mind that an analysis of Poiseuille flow between concentric cylinders was undertaken. When the radii of the cylinders are nearly the same, we have plane-Poiseuille motion; whereas it can be argued that a vanishing inner cylinder implies the pipe (Hagen–Poiseuille) motion. The results of the analysis of this problem give a not unexpected monotonic variation between the two limits. As the inner cylinder is reduced in size, the maximum value of the velocity shifts toward the inner cylinder, and the profile leans increasingly toward this cylinder. The marked increase in stability could be associated with an effect of the decreasing inner radius or perhaps with the skewing of the profile. To check this latter possibility, we generated a one-parameter family of increasingly skewed profiles (exact variable viscosity solutions of the Navier–Stokes equations) and analyzed the Orr–Sommerfeld stability of these. This stability analysis showed that the profiles which were deliberately skewed in annuli with fixed radius ratios exhibited an increased stability of the same general nature as that associated with reduction in size of the inner cylinder for the Poiseuille motion. A similar result has been found by Fu[5] for a sequence of profiles which are required to vanish at the wall (cf. Potter[6]) and are continuously deformed from Poiseuille flow to plane Couette flow. It would seem that the absolute stability which linear theory associates with plane-Couette and Hagen–Poiseuille motions is not a singular result but represents a limit result for profiles which increasingly depart from a least stable "symmetric" form.

The variable viscosity profiles are also more stable as they lean toward one wall or the other. But these

* Present address: Nuclear Engineering Department, The University of Tennessee, Knoxville, Tennessee.

[1] Linear theory, when it has meaning, gives sufficient conditions for instability. By "linear stability" we mean stability against disturbances of infinitesimal amplitude.

[2] C. C. Lin, *The Theory of Hydrodynamic Stability* (Cambridge University Press, London, 1955), Chap. 3.

[3] G. M. Corcos and J. R. Sellars, J. Fluid Mech. 5, 97 (1959).

[4] A. E. Gill, J. Fluid Mech. 21, 503 (1965).

[5] T. S. Fu, Ph.D. thesis, University of Minnesota (1967).

[6] M. C. Potter, J. Fluid Mech. 24, 609 (1966).

profiles are such that when they are sufficiently skewed the cylindrical analog of a point of inflection appears at one wall and moves into the stream. Long before this happens, however, a second, higher-wavenumber, minimum appears on the neutral curve. As the profile is more skewed this second minimum gives the absolute minimum. The two minima of the Reynolds number have very different distributions of the Reynolds stress; the walls near which energy is added to and extracted from the basic motion, are roughly interchanged in these two distributions.

The results reported in the sequel are calculated from asymptotic analysis and by finite-difference techniques. The details of the asymptotic analysis are of independent interest, as they bear on integration procedures for the two-turning-point problem.[5-8] The results of these calculations are checked against the results of finite-difference calculations and found acceptable. This independent check on the results of the asymptotic analysis is necessary because the simple turning-point solutions used here have not been rigorously derived for the two-turning-point problem. The good agreement between the two results does suggest that the older and simpler asymptotic methods are adequate for neutral stability of bounded inviscidly stable, shear flow.

Since it is not possible to calculate eigenfunctions and Reynolds stresses from asymptotic theory without a correction for the singular inviscid solution, the finite-difference method was used to evaluate these. The Reynolds stress distributions can be almost completely explained, however, from mathematical arguments alone.

In our analysis the usual assumptions of linear theory including the normal mode decomposition of solutions

$$\mathbf{q}(r, \theta, z, t) = \mathbf{q}(r) \exp [i(\alpha z + n\theta - \alpha c t)]$$

are employed. Here the symbols have the conventional meanings, and $c = c_r + ic_i$, where $c_i > 0$ means instability. We treat only axially symmetric ($n = 0$) disturbances from the outset. This is a major restriction, since there is no cylindrical equivalent to Squire's theorem. Moreover, though the experiments of Leite[9] as well as those of Wehrmann and Willie,[10] have both seemed to indicate that nonsymmetric disturbances were damped more rapidly than axially symmetric disturbances, Fox, Lessen, and Bhat[11] have demonstrated that Hagen–Poiseuille flow is unstable to the first mode ($n = 1$) of azimuthally periodic disturbances. It is just this azimuthal mode ($\eta = 1$, $\alpha = 1.07$) which is associated with the energy stability limit.[12] Among all the kinematically possible velocity fields (these are solenoidal fields which are periodic in z and vanish at $r = a$ and $r = b$), the one which is most efficient in transferring energy from the basic motion to disturbance motion in the pipe is just this spiral mode. In the annulus, for all but the largest radius ratios the purely transverse modes ($n \geq 2$) give the energy functional its least value. However, purely transverse modes must decay with time if initially present[13] and, therefore, cannot represent exact growing or stationary solutions of the nonlinear Navier–Stokes equations. The purely transverse disturbances most dangerous from a kinematic-energetic point of view are dynamically inadmissible, but the transverse *component* of dynamically admissible nonlinear modes may be central for transition.

II. STEADY VISCOUS FLOW BETWEEN CONCENTRIC CYLINDERS

In this section we describe two families of velocity profiles, whose stability we shall examine in subsequent sections. The expression

$$\Psi = \eta \frac{d}{d\eta}\left(\frac{1}{\eta}\frac{dW}{d\eta}\right), \tag{1}$$

where W is the velocity normalized with its maximum value V and η a dimensionless radius, is also evaluated. $\Psi = 0$ is one necessary condition[14,15] for the flow to be inviscidly unstable; that is, there are no amplified disturbances to the inviscid, Orr–Sommerfeld equation if $\Psi \neq 0$.

A. Poiseuille Flow

The relevant steady-flow solution is given by

$$W^* = \frac{(p_1 - p_2)}{4\mu l}\left(a^2 - r^{*2} + \frac{(b^2 - a^2)}{\ln (b/a)} \ln \frac{r^*}{a}\right), \tag{2}$$

[7] T. S. Chen, D. D. Joseph, and E. M. Sparrow, Phys. Fluids 9, 2519 (1966).
[8] W. Reid, in *Basic Developments in Fluid Dynamics*, M. Holt, Ed. (Academic Press Inc., New York, 1965), p. 249.
[9] R. J. Leite, J. Fluid Mech. 5, 81 (1959).
[10] O. Wehrmann and R. Wille, in *Boundary Layer Research Symposium Freiburg, 1957* (Springer-Verlag, Berlin, 1958), p. 387.
[11] J. A. Fox, M. Lessen, and W. A. Bhat, Phys. Fluids 11, 1 (1968).
[12] D. D. Joseph and S. Carmi, Quart. Appl. Math. (to be published). The most dangerous mode is not associated with the stream-wise disturbances (Re = 180) considered by Orr but with azimuthal disturbances proportional to cos θ (Re = 81.49). Stability to periodic disturbances of any magnitude is guaranteed for Re < 81.49.
[13] D. D. Joseph and L. N. Tao, J. Appl. Mech. 30, 147 (1963).
[14] S. Chandrasekhar, *Hydrodynamic and Hydromagnetic Stability* (Oxford University Press, London, 1961), p. 361.
[15] N. Gregory, J. T. Stuart, and W. S. Walker, Phil. Trans. Roy. Soc. London A248, 155 (1955).

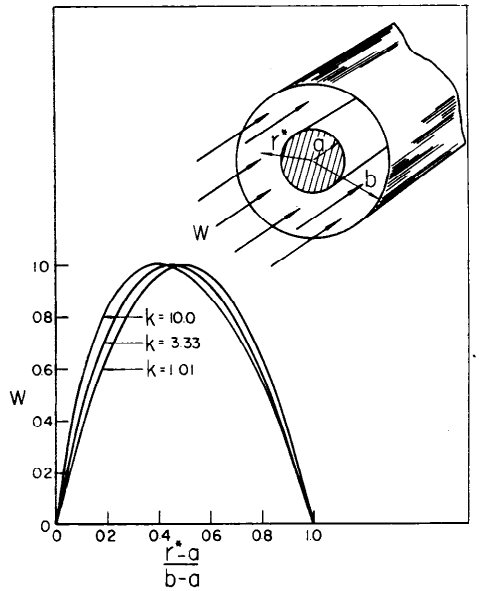

FIG. 1. Velocity distribution for Poiseuille flow. The velocity profile leans farther toward the inner cylinder as $k = b/a$ increases. The profile for $k \to \infty$ is the half-parabola associated with Hagen–Poiseuille flow.

where W^* is the axial flow and r^*, a, and b are the generic, inner, and outer radius, respectively. In dimensionless variables this is rewritten as

$$W = \frac{1 - \eta^2 + \eta_M^2 \ln \eta^2}{1 - \eta_M^2 + \eta_M^2 \ln \eta_M^2},$$

where

$$\eta = r^*/a = r(k-1)/2, \qquad \eta_M^2 = (k^2 - 1)/\ln k^2, \qquad k = b/a.$$

The graph of $W(\eta)$ is shown in Fig. 1.

We note that in the open region $(a, b]$

$$\lim_{a \to 0} W^* \to (p_1 - p_2)(b^2 - r^{*2})/4\mu l.$$

It follows that the velocity tends to the Hagen–Poiseuille values, but not uniformly. The influence on the flow of the small cylinder on which the velocity vanishes becomes increasingly less significant, because the force on the fluid per unit length of inner cylinder

$$2\pi a \tau_{rz} = \frac{\pi(p_1 - p_2)}{2l}\left[(b^2 - a^2)/\ln (b/a) - 2a^2\right]$$

tends to zero with a.

On the other hand,

$$\lim_{a \to \infty} W^* = \frac{(p_1 - p_2)}{4\mu l} y(y - 2d), \qquad b - a = 2d, \qquad r^* = a + y.$$

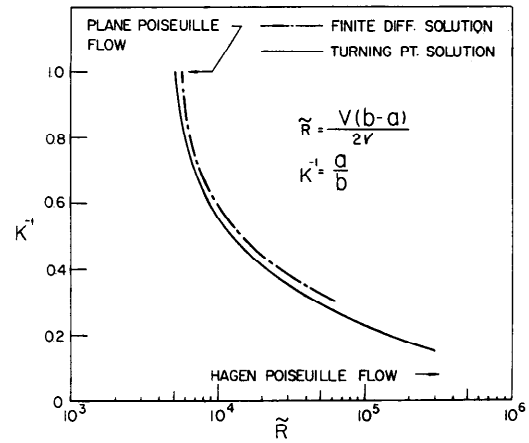

FIG. 2. Stability boundary for Poiseuille flow with the radius ratio k as a parameter. Plane–Poiseuille flow and Hagen–Poiseuille flow are connected by a monotone variation of the critical Reynolds number $\tilde{R}$.

Hence, the velocity tends uniformly to plane-Poiseuille flow values as the gap size is decreased relative to the inner radius. Therefore, it is likely that the stability calculation will yield the plane-Poiseuille flow result ($R = Vd/\mu \cong 5800$) in the small gap (radius ratio unity) limit. The identification of Hagen–Poiseuille flow ($R \to \infty$) with the limit of infinite radius ratio is not so easily asserted, and we have not established it. However, it is difficult to imagine how the cylinder of vanishing area which can exert no force on the fluid can influence the flow. For this reason we anticipate, and our results are consistent with, this identification (see Fig. 2).

Flows which are described by Eq. (2) cannot be inviscidly unstable ($\Psi = 0$) because

$$\Psi = -\frac{(p_1 - p_2)}{\mu l}\frac{(k^2 - 1)}{(k-1)^2 \ln k} r^{-2} < 0.$$

We draw attention to the increasingly skewed appearance of the velocity profile as k is increased (see Fig. 1).

B. Skewed Profiles

In order to obtain a wide variety of velocity profiles without varying the geometry, we envision the fully developed flow of a liquid with a temperature-sensitive coefficient of viscosity, say oil. The following velocity distribution [Figs. 3(a) and 4(a)] is an exact solution of the equations of momentum and energy for an oil-like liquid which satisfies a viscosity-temperature relation of exponential form

$$W = \frac{\eta_M^2(\eta^\beta - 1) - \beta(\eta^{\beta+2} - 1)/(\beta + 2)}{\eta_M^2(\eta_M^\beta - 1) - \beta(\eta_M^{\beta+2} - 1)/(\beta + 2)}, \qquad (3)$$

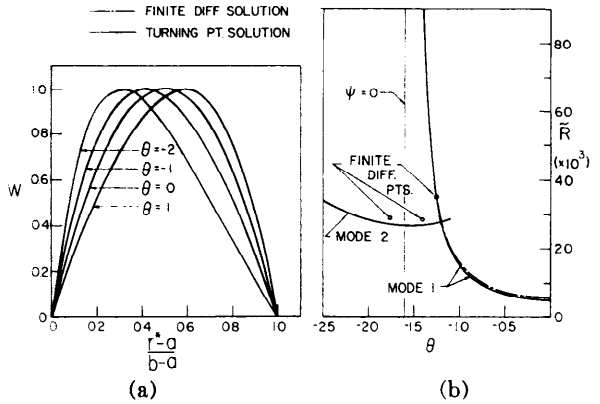

FIG. 3. (a) Velocity profiles for the variable viscosity flow [Eq. (3)] with $\theta = \beta \ln k$ and $k = 1.01$ as a parameter. The velocity profile leans farther toward one wall or the other as θ increases. (b) Stability boundaries for profiles of Eq. (3) with $k = 1.01$. For the parameter $\theta = 0$ the profile is almost symmetric and the motion is approximately of the plane-Poiseuille type. The stability boundaries are nearly symmetric around $\theta = 0$. The second-mode stability boundary extends farther into the first mode region but is difficult to trace in this region.

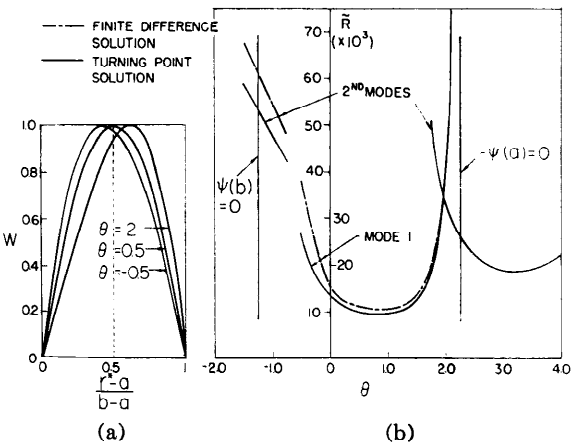

FIG. 4. (a) Representative velocity profiles for $k = 2$. (b) Stability boundaries for profiles of Eq. (3) with $k = 2$. The profiles which lean heavily to one wall or another are considerably more stable than those which are more nearly "symmetric." The double minima of the neutral curves which belong to the intersection region ($\theta = 2$) are shown in Fig. 5.

where β is the temperature parameter $(-1/\mu)\cdot(\partial\mu/\partial T)(T_b - T_a)/\ln k$, T the temperature, and

$$\eta_M^2 = \frac{\beta}{\beta + 2}\frac{(k^{\beta+2} - 1)}{(k^\beta - 1)}$$

is the root η_M of $0 = dW/d\eta$. The distribution $W(\eta)$ is such that

$$W(1) = W(k) = 0, \qquad W(\eta_M) = 1,$$

and

$$\Psi = \frac{\lambda^2}{2}[(\beta - 2)\eta_M^2 - \beta\eta^2]\eta^{\beta-2},$$

where $\lambda^2 = (p_1 - p_2)a^2/\mu_0 lV$ is the dimensionless pressure drop. When $\beta = 0$, we have constant viscosity. It is of little consequence that Eq. (3) is an exact solution. We do not perturb temperature and may regard Eq. (3) as an invention used to study the two-turning-point problem.

III. PERTURBATION EQUATIONS

We normalize all velocities with the maximum velocity V of the basic flow. A dimensionless length r, related to the radius r^* by

$$r = 2r^*/(b - a)$$

and a Reynolds number

$$R = V(b - a)/2\nu$$

are introduced into the governing, small perturbation equations written in cylindrical coordinates.

For axially symmetric disturbances the cylindrical equivalent of the Orr–Sommerfeld equation is

$$(W - c)L\omega - \Psi\omega = -\frac{i}{\alpha R}L^2\omega, \qquad (4)$$

$$\omega(r_1) = \omega(r_2) = \omega'(r_1) = \omega'(r_2) = 0,$$

where W is the normalized, basic-flow velocity, ω the amplitude of the radial component of the disturbance velocity, r_1 is the inner and r_2 the outer radius, and

$$L = \frac{d^2}{dr^2} + \frac{1}{r}\frac{d}{dr} - \frac{1}{r^2} - \alpha^2, \qquad A' = \frac{dA}{dr}.$$

This axially symmetric equivalent to the Orr–Sommerfeld equation can be analyzed in an extensive analog to plane-parallel flow. It is to this analysis that we now turn.

IV. ASYMPTOTIC SOLUTIONS

The asymptotic methods developed by Heisenberg,[16] Lin,[17] and Tollmien,[18] with minor modifications, may be applied to this problem. No essential difficulty arises from the nonsymmetry of the steady velocity profiles. We describe our treatment of the two-turning-point problem below.

A. Inviscid Solutions

Two inviscid solutions of Eq. (4) may be obtained (after Heisenberg[16]) by setting

[16] W. Heisenberg, Ann. Physik **74**, 577 (1924).
[17] C. C. Lin, Quart. Appl. Math. **3**, 117 (1945).
[18] W. Tollmien, Nachr. Kgl. Ges. Wiss. Gottingen 21 (1929).

$$\left.\begin{matrix}\omega_1\\ \omega_2\end{matrix}\right\} = \frac{(W-c)}{r}\begin{cases}h_0 + \alpha^2 h_1 + \cdots\\ k_1 + \alpha^2 k_3 + \cdots\end{cases}, \qquad (5)$$

where

$$h_0 = 1,$$

$$h_{2n+2} = \int_{r_{c_1}}^{r} \frac{\eta\, d\eta}{(W-c)^2} \int_{r_{c_1}}^{\eta} \frac{h_{2n}(r)(W-c)^2}{r}\, dr,$$

$$k_1 = \int_{r_{c_1}}^{r} \frac{\eta\, d\eta}{(W-c)^2},$$

$$k_{2n+3} = \int_{r_{c_1}}^{r} \frac{\eta\, d\eta}{(W-c)^2} \int_{r_{c_1}}^{\eta} \frac{k_{2n+1}(W-c)^2}{r}\, dr.$$

Because of the logarithmic singularities at r_{c_1} and r_{c_2} where $W = c$ [$W'(r_{c_1}) > 0$, $W'(r_{c_2}) < 0$], the proper path in the complex plane must be chosen so as to circumvent these singular points. The proper path is that one which goes below the first critical point (Tollmien[18]) and above the second one (Foote and Lin,[19] Potter[5]) in the complex r-r_c plane. The integrals used in Eq. (5) were evaluated numerically with the series truncated when n exceeded five.

B. Viscous Solutions

Our choice for viscous solutions follows as a consequence of the heuristic requirement that a viscous solution decays exponentially with distance from a wall.[20]

We designate the viscous solution near the inner wall as ω_3, that near the outer wall, as ω_4. The form of these viscous solutions then follows as an easy generalization of single-turning-point asymptotic analysis.

First, consider ω_3. The turning point approximation $\omega_3 \cong \chi_3$ for real c and $W(r_{c_1}) = W_{c_1}$ is

$$\chi_3 = \int_{\infty}^{z_1} dr \int_{\infty}^{r} \nu^{\frac{1}{2}} H_{\frac{1}{3}}^{(1)}[\tfrac{2}{3}(i\nu)^{\frac{3}{2}}]\, d\nu, \qquad (6)$$

with

$$z = (\alpha R W'_{c_1})^{\frac{1}{3}}(r - r_{c_1}),$$

where

$$\begin{aligned} W - c &= |W-c|\, e^{-i\pi}, \\ r - r_{c_1} &= |r - r_{c_1}|\, e^{-i\pi}, \end{aligned} \qquad r < r_{c_1},$$

$$\begin{aligned} W - c &= |W-c|, \\ r - r_{c_1} &= |r - r_{c_1}|, \end{aligned} \qquad r > r_{c_1}.$$

The turning-point approximation (6) is valid in the limit $\alpha R \to \infty$, $z \neq 0$ fixed, with an error $O(\alpha R)^{-\frac{1}{3}}$. These solutions are valid for complex arguments in the sector $-\frac{7}{6}\pi < \arg(r - r_{c_1}) < \frac{1}{6}\pi$.

Approximations to ω_4 are constructed by techniques identical with those used to obtain ω_3, but one must be careful with phases. The result for real c,

$$W'(r_{c_2}) = |W'_{c_2}|\, e^{-i\pi}$$

follows: χ_4 is obtained from Eq. (6) by replacing z_1 with z_2, where

$$z = (\alpha R\, |W'_{c_2}|)^{\frac{1}{3}} e^{-i\pi}(r - r_{c_2}),$$

and

$$\begin{aligned} W - c &= |W-c|, \\ r - r_{c_2} &= |r - r_{c_2}|\, e^{i\pi}, \end{aligned} \qquad r < r_{c_2},$$

$$\begin{aligned} W - c &= |W-c|\, e^{-i\pi}, \\ r - r_{c_2} &= |r - r_{c_2}|, \end{aligned} \qquad r > r_{c_2}.$$

The remarks concerning the validity of the viscous solutions apply here as well except that the complex region in which χ_4 is valid is

$$-\tfrac{1}{6}\pi < \arg(r - r_{c_2}) < \tfrac{7}{6}\pi.$$

C. Boundary Conditions

We have now four solutions: two inviscid solutions (ω_1, ω_2) valid throughout the region and two viscous solutions (χ_3, χ_4). Of the viscous solutions only one at each wall is compatible with the condition that the viscous solution should decay from the wall. The consequence of this remark and the boundary conditions is the indicial equation

$$D = \begin{vmatrix} \omega_{11} & \omega_{21} & \chi_{31}/\chi'_{31} & 0 \\ \omega'_{11} & \omega'_{21} & 1 & 0 \\ \omega_{12} & \omega_{22} & 0 & \chi_{42}/\chi'_{42} \\ \omega'_{12} & \omega'_{22} & 0 & 1 \end{vmatrix} = 0. \qquad (7)$$

It is convenient for numerical calculations to replace the viscous terms in Eq. (7) with terms which depend on Tietjens function. Thus, we have

$$\frac{\chi_{31}}{\chi'_{31}} = (r_1 - r_{c_1})F(-z_1). \qquad (8)$$

The ratio χ_{42}/χ'_{42} is obtained from Eq. (8) by substituting subscript 2 for 1. The series representation of Tietjens function[7] is convenient for calcula-

[19] J. R. Foote and C. C. Lin, Quart. Appl. Math. 8, 265 (1950).

[20] The solution which grows exponentially is ordinarily designated with a subscript four, carried along and finally thrown away. We discard it from the outset. The solution we designate with a subscript four should not be confused with this discarded growing solution.

tion, because the convergence is rapid enough to make a fresh calculation of the ratios (8), etc., feasible for each eigenvalue computation. The iterative procedure used to solve Eq. (7) is described in Mott's thesis.

In order to obtain an independent check on the results obtained by asymptotic analysis, a separate program of numerical analysis was undertaken. A finite-difference method, used first by Thomas[21] and subsequently by Kurtz and Crandall,[22] and then by Tsou[23] was employed. A description of the finite-difference program can be found in Mott's[24] thesis. We could not always obtain convergent finite-difference results for Reynolds numbers in excess of 50 000.

V. STABILITY OF POISEUILLE FLOW BETWEEN CYLINDERS

This section summarizes our results relative to the stability of Poiseuille flow in annular ducts. The relevant data may be found in Fig. 2 (see Mott[24] for tables and neutral curves). In this data the tilde overbar quantities are values of the parameters belonging to the minimum critical value of the Reynolds number for a fixed k, i.e.,

$$\tilde{R}(k) = R(\tilde{\alpha}, \tilde{c}, k) = \operatorname*{Min}_{\alpha} R(\alpha, c, k).$$

The following observations merit special attention:

(1) Asymptotic and finite-difference solutions are in reasonable agreement over the range in which they can be compared. The accuracy of the asymptotic solutions is conservatively estimated by Fig. 2. This gives the locus of the nose of neutral curves for different radius ratios. The asymptotic and finite-difference solution are most different near the nose and tend to coalesce for large R.

(2) The stability limit increases montonically with the radius ratio from the known value for Poiseuille flow in channels toward infinity in the Hagen–Poiseuille flow limit (Fig. 2). We call attention to the increased skewing of the velocity profiles for larger radius ratios. The limit profile is Hagen–Poiseuille flow with a spike at $r = 0$ and the absolute stability of Hagen–Poiseuille flow is evidently a limit result of a sequence of increasingly skewed profiles (cf. Sec. VI).

[21] L. H. Thomas, Phys. Rev. 91, 780 (1953).
[22] E. F. Kurtz and H. C. Crandall, J. Math. Phys. 41, 264 (1962).
[23] F. K. Tsou, Ph.D. thesis, University of Minnesota (1965).
[24] J. E. Mott, Ph.D. thesis, University of Minnesota (1966).

VI. SKEWED PROFILES IN ANNULAR DUCTS OF FIXED RADIUS RATIO

There are two results which follow from the study of the $\theta(= \beta \ln k)$ family of profiles represented by Eq. (3). The first of these duplicates a result of the previous section, namely, that the critical value of the Reynolds number $\tilde{R}_1(\theta)$ increases rapidly as the profile is skewed far toward one wall or the other. The second result is the appearance of a second minimum in the curve of neutral stability. This minimum in the neutral curve for plane-Poiseuille flow, dominates the stability of the θ family of velocity distributions with sufficiently skewed profiles.

It is convenient to discuss these two minima separately. For this purpose we define two critical eigenvalues $\tilde{R}_1(\theta)$ and $\tilde{R}_2(\theta)$ which correspond to these two minima and which we will call modes one and two.

A. Mode-One Instabilities

This instability is of the viscous type studied by Tollmien[18]. We have studied this instability as a function of the parameter θ for $k = 1.01$ and 2.0. The first of these is essentially a flow in a plane channel which, when $\theta = 0$, is nearly plane-Poiseuille flow. Our results relative to this instability are represented in Figs. 3(b) and 4(b). These conclusions are suggested by our data: (1) The mode-one instabilities over the range of values calculated are confined to values of θ for which $\Psi \neq 0$. (2) The mode-one instability occurs at the smallest value of $\tilde{R}_1$, for symmetric, or nearly symmetric profiles. For $k = 1.01$ the symmetric profile is defined roughly by $\beta \simeq \theta_s \simeq 0$ [see Fig. 3(a)] whereas for $k = 2.0$ a "symmetric" profile may be defined at $\theta_s = \beta_s \ln 2 \simeq 0.5$ so that $\tilde{R}_1(\theta - \theta_s)$ is an increasing function of $|\theta - \theta_s|$ [see Figs. 4(a) and 4(b)]. Profiles which lean heavily toward one wall or the other are more stable than "symmetric" profiles [Figs. 3(a), 4(a)].

We note that $\tilde{R}_1$ is not the smallest value of R for all values of θ. For certain values the second mode with critical eigenvalues $\tilde{R}_2$ may be smallest. We now consider this second mode.

B. Mode-Two Instabilities

The existence of this second viscous mode was established by direct calculation from both finite-difference and asymptotic solutions. The results for $k = 1.01$ and $k = 2.0$ are summarized in Figs. 3–5. Further results, including dispersion relations, may be found in Ref. 24.

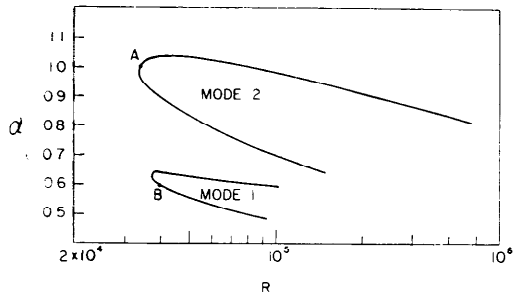

FIG. 5. Neutral curves for the two modes belonging to $k = 2.0$ and $\theta = 2.0$. For point A, $k = 2.0$, $\theta = 2.0$, $\alpha = 1.01$, $c = 0.2115$, and $R = 32\,600$. For point B, $k = 2$, $\theta = 2.0$, $\alpha = 0.6$, $c = 0.130$, and $R = 41\,800$.

Second-mode instabilities exist and are present for both positive and negative values of θ. Although the second mode passes through values of θ for which the necessary condition for inviscid instability, $\Psi = 0$, is satisfied, it also contains a set of θ values for which $\Psi \neq 0$ and hence cannot be an inviscid instability.

Our understanding of the two modes is enhanced by an examination of the distribution of Reynolds stresses which is undertaken in the next section.

VII. REYNOLDS STRESSES AND ENERGETICS OF THE DOUBLE MINIMUM

We restrict our attention to the eigenvalues associated with points A and B of Fig. 5. The distribution of the eigenfunctions belonging to these two points is given in Figs. 6 and 7. We have no comment about these eigenfunctions other than to echo the often made homage to the difficulty of this problem so plainly evident in the graphs of the imaginary part of $u(r)$ (Fig. 7).

Next consider the distribution of Reynolds stress [Figs. 8(a) and 9(a)] and the distribution of the energy supply [Figs. 8(b) and 9(b)]. Some properties of the Reynolds stress and energy supply are known.

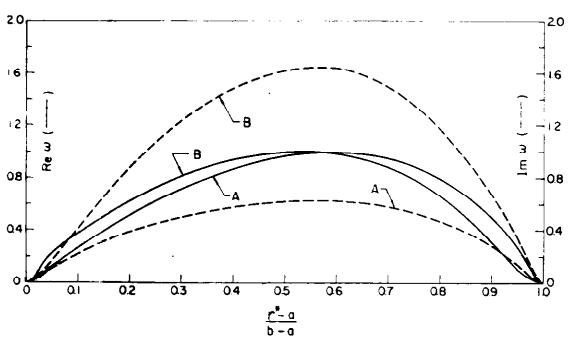

FIG. 6. Real and imaginary parts of the radial amplitude $\omega(r)$ corresponding to points A and B of Fig. 5.

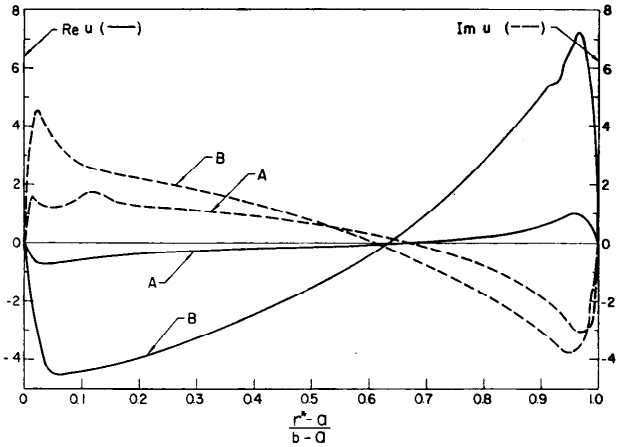

FIG. 7. Real and imaginary parts of the axial amplitude $u(r)$ [$= (i/\alpha r)\, d(\omega r)/dr$] corresponding to points A and B of Fig. 5.

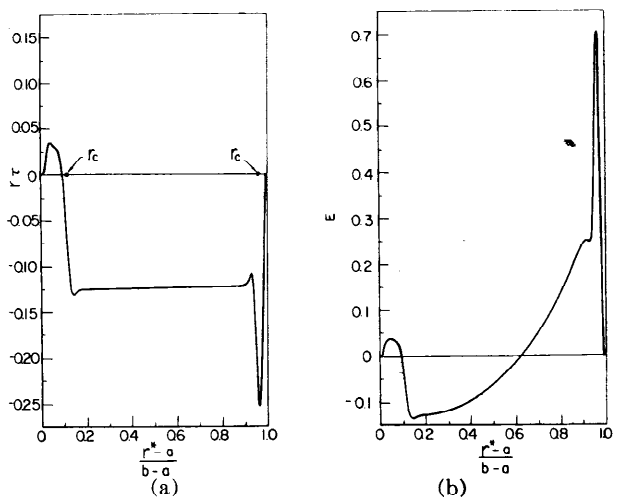

FIG. 8. (a) Reynolds stress distribution for flow corresponding to point A of Fig. 5. (b) Energy supply for point A of Fig. 5. Where E is positive, energy is transferred from the basic motion to the disturbance motion.

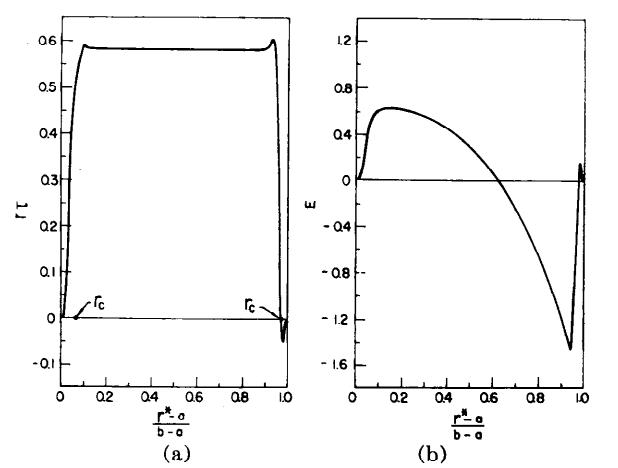

FIG. 9. (a) Reynolds stress distribution for flow corresponding to point B of Fig. 5. (b) Energy supply for point B of Fig. 5.

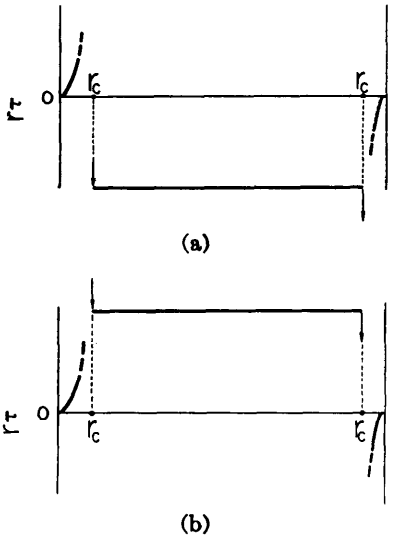

FIG. 10. The disturbance boundary-layer analysis of Lin[25] and the jump condition for the Reynolds stress imply conditions (13). These conditions do not determine the sign or magnitude of the Reynolds stress in the inviscid center. If the sign of the Reynolds stress is assumed to be positive we have the situation sketched in Fig. (a) whereas a negative Reynolds stress implies the sketch in Fig. (b). Both distributions occur [see Fig. 8(a) and 9(a)]. A good qualitative picture of these distributions (which were calculated numerically by finite differences) follows also upon completion of the sketches of Fig. 10 as smooth curves in the most obvious way.

It seems appropriate to review the analysis leading to these properties.

Let ω^* be the conjugate of ω. Then one may obtain from Eq. (4) an equation for the Reynolds stress:

$$\hat{\tau} = -(\rho/\lambda)\int_0^{\lambda} \mathrm{Re}\,(q_r)\,\mathrm{Re}\,(q_z)\,dz,\quad \lambda = \text{wavelength},$$

$$\frac{(W-c_r)}{r}\frac{d}{dr}(r\tau) - c_i(\omega^* L\omega + \omega L\omega^*) = -(\alpha R)^{-1}(\omega^* L^2\omega + \omega L^2\omega^*), \qquad (9)$$

where

$$i\tau = \omega^*\frac{d\omega}{dr} - \frac{d\omega^*}{dr}\omega = \frac{4i\alpha\hat{\tau}}{\rho V^2}\exp\left[\frac{4c_i\alpha l V}{(b-a)}\right].$$

First, let $c_i = 0$ (neutral oscillation), multiply Eq. (9) by r and integrate across the annulus

$$\int_1^2 \frac{d}{dr}[(W-c_r)r\tau]\,dr - \int_1^2 r\tau\frac{dW}{dr} = -(\alpha R)^{-1}\int_1^2 r(\omega^* L\omega + \omega L^2\omega^*)\,dr.$$

The first of these integrals vanishes by virtue of the boundary conditions and one finds, after an integration by parts, that

$$\frac{1}{\alpha R} = \frac{\int_1^2 E\,dr}{2\int_1^2 r\,|L\omega|^2\,dr},$$

where $E = r\tau\,dW/dr$ is the energy supply.

The energy transfer between the basic and disturbed motion depends upon the sign of E; when positive, energy is transferred from the basic motion to the disturbance motion. It is apparent that E vanishes at a rigid wall.

Lin[25] has shown that near the wall ($W \ll c_r$) $E > 0$. Hence τ must be positive near the inner wall ($r = a$) and negative near the outer wall ($r = b$).

More can be said about the distribution of τ by considerations following from inviscid theory. One expects that viscosity is important only in the neighborhood of the walls and in a neighborhood of the critical layer. In the interior, the flow is largely inviscid. Hence, $r\tau_I$ satisfies

$$\frac{W-c_r}{r}\frac{d}{dr}(r\tau_I) - c_i(\omega_I^* L\omega_I + \omega_I L\omega_I^*) = 0$$

obtained from Eq. (9), by letting $(\alpha R)^{-1} \to 0$. Similarly, Eq. (4) becomes $L\omega_I = \Psi\omega_I/(W-c)$ so that by combining we find

$$\frac{d(r\tau_I)}{dr} = \frac{2c_i r\Psi\,|\omega_I|^2}{|W-c|^2}. \qquad (10)$$

Thus, it is found[19] that in the limit as c_i approaches zero

$$r\tau_I \to \text{const} \qquad (11)$$

for all r on the domain of W such that $W - c_r \neq 0$.

The roots of the equation $W - c_r = 0$ define the position of the critical layer. It is also possible to calculate from Eq. (10) the magnitude of the jump discontinuity at each critical layer.[19] One finds that

$$[\tau_I]_{r_c-\epsilon}^{r_c+\epsilon} = \frac{2\Psi_c\,|\omega_c|^2\,\pi}{|dw/dr|_c}, \qquad (12)$$

where $0 < \epsilon \to 0$ and all quantities are evaluated at a critical layer. Equation (12) holds at both critical layers. Since $\Psi_c < 0$ on the domain of W the jump is negative at both critical layers.

Then, on analytical grounds, we expect that

(1) *τ is positive as $r \to a$ and negative as $r \to b$,*

(2) *$r\tau \cong r\tau_I =$ const in the region between the critical layers,* (13)

(3) *$[r\tau_I]_{r_c-\epsilon}^{r_c+\epsilon} \leq 0$ at each critical layer.*

[25] C. C. Lin, Proc. Natl. Acad. Sci. (U. S.) 40, 741 (1954). A proof of this result is also given in Ref. 2, p. 54.

The sign and magnitude of $r\tau_I$ in the center inviscid region is not determined by these considerations.

With these considerations in mind we anticipate that the shear stress distribution will have the features shown in either Figs. 10(a) or (b) depending on the sign of $r\tau_I$. A qualitative picture of the true distribution of $r\tau$ [Figs. 8(a) and 9(a)] follows easily by completing the sketches as smooth curves in the most obvious way.

The graphs of the energy supply [Figs. 8(b) and 9(b)] clearly demonstrate that, in asymmetric flow, there exist large regions where the energy supply is negative and the disturbance motion returns energy to the basic flow. This feature, which tends to stabilize the motion, cannot be present to any appreciable extent in symmetric flows since τ_I must be zero in order for their eigenfunctions to be symmetric.

ACKNOWLEDGMENTS

This work was supported by a National Science Foundation Faculty Fellowhip granted one of the authors, Mott, by a National Aeronautics and Space Administration Grant (NGR-24-005-065) to the Space Science Center of the University of Minnesota, and by National Science Foundation Grants (GK1613), University of Tennessee and (GK1838) to the University of Minnesota. Use of the computer granted by the Computing Center of the University of Minnesota is also acknowledged.